LOI12-16-005

Target Helicity Correlations in GlueX

Letter of Intent

D. Keller,[‡]
University of Virginia, Charlottesville, VA 22903

F.J. Klein,
The Catholic University of America, Washington, DC 20064

W.K. Brooks,
Universidad Tecnica Federico Santa Maria, Valparaiso, Chile

C. Keith,
Thomas Jefferson National Accelerator Facility, Newport News, VA 23606

[‡]Contact

Abstract

We express interest in an experimental program to measure a broad range of spin observables in the photon energy between 5 and 9 GeV using the existing GlueX detector package in Hall D along with a new frozen spin target of polarized protons and deuterons. The polarized target will be capable of both longitudinal and transverse polarizations, so that in conjunction with linearly and circularly polarized photons, a complete set of spin observables can be determined in a single experiment, including single polarization and beam-target, target-recoil, and beam-recoil double-polarization asymmetries, as well as tensor polarized observables, and initial state helicity correlations in possible exotic state hadrons. This experiment is complimentary to previously proposed GlueX experiments, providing additional information to be used to determine complete isospin amplitudes and assist the search for exotic state mesons. Investigation into these possibilities could potentially lead to a series of polarized target experiments enhancing the on-going investigation into spin structure as well as the exotic state contributions.

Contents

1 Background and Motivation

Polarized observables exhibit very rich structure, reflecting the degree of complexity in dynamics adding considerable sensitivity and information in each measurement. This additional information on the various contributions leading to the final state is crucial and will need to be fully exploited in attempts to understand exotic contributions.

Photo-excitation of the nucleon as seen in the hadronic spectrum provides the quintessential tool for probing the quark and gluonic degrees of freedom, the nature of the confinement mechanism, possible gluon-gluon interactions, and the missing resonances. Exotic hybrid mesons manifest gluonic degrees of freedom, and their detailed spectroscopy will provide the precision data necessary to test assumptions in lattice QCD and the specific phenomenology leading to confinement. The use of polarized photon beams with polarized targets provides the most information and comprehensive set of constraints to assist in the search of exotic mesons as well as an understanding of their backgrounds.

In general, higher mass resonances can overlap with significant interfering backgrounds from u-channel processes. Multivariate extraction techniques and detailed partial-wave analyses are invaluable, as are the constraints provided by the polarization of the target nucleons. The ideal frame-work would account for the coupling between the various meson-decay channels using as many polarized observables as can be achieved. A comprehensive investigation of amplitudes and phase transitions is required for both the meson and baryon spectrum, which is chiefly determined from πN reactions to assist in the deconvolution of the spectrum in the search for and study of the pattern of gluonic excitation in the meson spectrum. Using polarized target data with unpolarized target data is the most thorough way to explore the spectrum for exotic states. The measurement of double spin polarization asymmetries can reveal information on the nucleon hidden structure, hadron photoproduction dynamics, and exotic hadron property. Exploring the asymmetries of Compton scattering over broad angular coverage is now much more realistic with the Hall-D optimized trigger using Boosted Decision Tree pattern recognition. It is likely to see a very strong signal in A_{NN} at the charm threshold in polarized $\gamma p \to \gamma p$ at large angles when both beam and target are polarized transverse to the beam direction. This could signify an exotic state in even the simplest of reactions [1]. There are many channels to explore with polarized observables.

Enhanced dynamics have been seen near the heavy-quark thresholds where a large 4:1 transverse-transverse spin correlation A_{NN} is observed in large-angle elastic proton-proton scattering at $\sqrt{3}$ GeV and $\sqrt{5}$ GeV. These energies correspond to the strange and charm thresholds in the two-baryon system. The observed strong spin correlations are consistent with the formation of $J = L = S = 1$ octoquark resonances near the heavy quark pair thresholds. In photoproduction, the production energy can not be wasted at threshold, so all three valence quarks of the target nucleon must interact coherently within the small interaction volume of the heavy quark production subprocess. The same strong spin correlations can be studied with polarized photons and a polarized proton target for the Hall-D photon energy. In the case of threshold charm photoproduction on a deuteron, all color configurations of the six valence quarks will be involved at the short-distance scale $1/m_c$ [2]. Thus the exchanged gluons can couple to a color-octet quark cluster and reveal the "hidden-color" part of the nuclear wave function [3].

Polarization observables can be instrumental for separating of the exotic waves. The expected

dominance of the one-pion-exchange which fixes naturality in the t-channel for some typologies can enable, by means of polarization observables, discrimination between naturalities of the resonances produced. If there are limitations in the partial wave analysis (PWA) it is sometimes possible to find maxima in the angular distributions of the decay products which are dominated by a single resonance of interest.

The enhancement of the hadronic interactions at threshold implies that new types of charm-based resonances may form in photoproduction in the available energy range. Some of the possibilities are the J/ψ-nucleon resonances at threshold in reactions such as $\gamma p \to [J/\psi p]$, $\gamma p \to [J/\psi p]\gamma$, $\gamma p \to [J/\psi]\pi^+$, and with the deuteron target $\gamma d \to \bar{D}^0 + [\Lambda_c n]$ and $\gamma d \to [\Lambda_c] + [\bar{D}^0 n]$ reactions. Another possibility is the octoquark $|uuduudc\bar{c}>$ in γd. In each case, resonance formation implies strong spin correlations.

There are many polarized observables that can be acquired with the combination of a polarized photon and a polarized nucleon target. These observables are important for the development of a complete understanding of the production mechanisms of the various resonances. As an example, the $\Lambda(uds)$ caries its polarization in the strange quark, with a small contribution from the (ud) diquark, where the polarization mechanism of the $\Xi((u/d)ss)$ may come from the valence quark (u/d) instead of the (ss) diquark. The $\Xi(1320)$ can be photoproduced on a polarized nucleon target which can then be used to study the different contributions of the valence quarks to the nucleon polarization. Polarized beam/target data can be compared to other GlueX experiments without beam/target polarization. Measurements of the in-plane polarization of the $\Xi^-(1320)$ can be used to differentiate between polarization and production mechanisms.

Investigations of the multi-strange hyperons are still laking. There are still far fewer Ξ resonances than Δ resonances, which under the flavor SU(3) symmetry leads to the notion that there is still much to discover. This would likely take an anti-kaon beam or a long running photoproduction experiment in combination with multivariate analysis techniques and trigger, all of which may be feasible in Hall-D.

Considering the photoproduction reaction $\gamma N \to KK\Xi$, a measure of the transverse spin-transfer can be determined by measuring both the double-polarization observable K_{yy} and the photon-beam asymmetry Σ [4]. These observables are related to the parity of the Ξ resonance by

$$\pi_\Xi = \frac{K_{yy}}{\Sigma}.$$

This same technique can be used to study the parity of the Ω hyperon in the reaction $\gamma N \to KKK\Omega$. This can also be generalized to the Ξ of higher spin and to the polarization observables in Ξ photoproduction [5].

1.1 Overview

In the following letter of intent, we discuss just some of the interesting polarized observables that can come from a polarized or unpolarized photon beam on a polarized target. There is much to learn in the photon energy range of 5-9 GeV, the approved GlueX experiments E12-06-102, E12-13-003, and conditionally approved experiment C12-12-002 will significantly add to our knowledge base. To a large extent, these experiments must run in order to know exactly what decay

channels will benefit most by using a polarized target. At this stage, it is clear that there is independently much physics to come from using a polarized target as well as using polarized observables as a compliment to the proposed exotic state search in GlueX and by enhancing the level of information on background and competing channels. The goal here is to motivate the construction of a polarized target to be used in GlueX for a number of helicity configurations of the proton and deuteron to be part of an ongoing target-spin physics program in Hall-D.

2 Polarization Observables

In the search for exotic mesons polarized target data should be taken to acquire the most information on the amplitudes and phase contributions seen in the spectrum. Confirmation of any $J^{p,c}$ states in the un-polarized target GlueX runs will be critical and polarized target information can be used to provide additional constraints. This information can also be helpful in the separation of exotics from non-trivial gluonic constructions of non-exotic hybrid mesons. The polarized target observables help to make a more *complete* measurement for a given topology. The masses and quantum numbers are essential in a measurement of an exotic states but also phenomenology that may arise from NN*-exotic couplings. An intimate understanding of the background in require with many channels adding constrains over phase space through the study of the polarized observables. As an example, the polarized observables for the processes $\gamma N \to \pi\pi N$ and $\pi N \to \pi\pi N$ were developed [6] using both a helicity and hybrid helicity-transversity basis. Such observables are crucial if processes that produce final states consisting of a spin-1/2 baryon and two pseudoscalar mesons are to be fully investigated in meson/baryon spectroscopy. In the general case, the S, P_0, P_+, and P_- amplitudes and their relative phases depend on the nucleon helicities. Without using a polarized target, these partial waves cannot be deduced from the moments without further assumptions [7, 8]. Without polarization data, there are no unambiguous solutions and additional assumptions are necessary. For photoproduction, the one pion exchange mechanism dominates which prefers spin flip at the nucleon vertex. Under these conditions, the rank of the spin-density matrix is reduced to one and all density matrix elements can be fixed. In [9] it was thus assumed that for small values of t, the proton spin-flip amplitude is dominant. More generally speaking, it was assumed that the $\pi\pi$ phase does not depend on the projection of the orbital angular momentum onto the flight direction with which it is produced (phase coherence) and that the ratio of flip and non-flip amplitudes is universal (spin coherence). For large t, neither phase nor spin coherence is granted, and feedthrough of higher partial waves into the scalar wave cannot be excluded without exploiting a polarized target. The greatest amount of information will come out of GlueX by searching for exotic hadron states while mapping the coupled-channel background. This is best done with wide kinematic coverage and many polarization observables. In the next few section we discuss some of the critical polarized observables achieved using various configuration of the polarized target.

Photon			T			R				+	
	-	-	-	-	x'	y'	z'	x'	x'	z'	z'
	-	x	y	z	-	-	-	x	z	x	z
Unpolarized	σ_0	0	T	0	0	P	0	$T_{x'}$	$-L_{x'}$	$T_{z'}$	$L_{z'}$
Linearly Pol.	$-\Sigma$	H	$(-P)$	$-G$	$O_{x'}$	$(-T)$	$O_{z'}$	$(-L_{z'})$	$(T_{z'})$	$(-L_{x'})$	$(-T_{x'})$
Circularly Pol.	0	F	0	$-E$	$-C_{x'}$	0	$-C_{z'}$	0	0	0	0

Table 1: Polarization observables in photoproduction of pseudoscalar mesons. The entries in brackets denote polarization observables which also appear elsewhere in the table. Here T is target, R is recoil, and + is target and recoil.

2.1 Pseudoscalar Mesons

Photoproduction of pseduoscalar meson can be used to obtain a large number of polarized target observables on both the polarized proton and neutron targets. The two spin states of the photon and the nucleon lead to four complex helicity amplitudes that determine single-pseudoscalar ($J^\pi = 0^-$) meson production from the neutron target and four from the proton target. There are eight quantities to be determined for each target isospin by measuring different observables. In addition to the unpolarized cross section, there are three single-spin asymmetries accessed by polarizing the beam (Σ), the target (T), or the recoiling baryon (P), as well as three sets of double-polarization asymmetries corresponding to the beam-target (BT), target-recoil (TR), and beam-recoil (BR) combinations. A complete data set that eliminates discrete ambiguities requires a minimum of eight observables which include the unpolarized cross section, the single-spin asymmetries (Σ,T,P), and four double-polarization asymmetries, at least one involving recoil polarization. Ideally even a larger number of different observables is desirable to mitigate the effects of systematic uncertainty in a PWA. Triple-polarization data for single-pseudoscalar meson production can provide additional determination of other observables. In the following section just a few are mentioned.

2.1.1 Polarized Proton Target

Circular polarized beams can be used to measure the E beam-target asymmetry and the $C_{x'}$ and $C_{z'}$ beam-recoil asymmetries (in-plane recoil components), and linearly polarized photon beams can be used to measure the single-spin beam asymmetry defined as Σ, the G beam-target asymmetry, the $O_{x'}$ and $O_{z'}$ beam-recoil (in-plane component) asymmetries, and the single-spin target asymmetry T, a beam-recoil observable. Combining all beam polarization states will provide measurements of the Λ recoil single-spin asymmetry, P, and the target-recoil observables $L_{x'}$ and $L_{z'}$ (in-plane components). Finally, triple beam-target-recoil measurements with linearly polarized photons will access the transverse-Target-Recoil asymmetries $T_{x'}$ and $T_{z'}$.

The polarization observables [10] in photoproduction of pseudoscalar mesons are related to the photon beam, target, and recoil polarization states in Table 2.1.1. There are 16 different polarization observables for real photon experiments. The differential cross section can be classified by

3 classes of polarization experiments. For a polarized photon with a polarized proton target, the cross section is expressed as

$$\begin{aligned}\frac{d\sigma}{d\Omega} &= \sigma_0[1 - P_{lin}\Sigma\cos 2\varphi \\ &+ P_x(-P_{lin}H\sin 2\varphi + P_\lambda F) \\ &- P_y(-T + P_{lin}P\cos 2\varphi) \\ &- P_z(-P_{lin}G\sin 2\varphi + P_\lambda E)],\end{aligned} \tag{1}$$

where σ_0 is the unpolarized differential cross section, P_{lin} is the transverse photon polarization, P_λ is the (right-handed) circular photon polarization, and ϕ is the angle between photon polarization vector and reaction plane. The polarization states of the target proton and recoiling baryon are denoted by $P_{x,y,z}$ and $R_{x',y',z'}$ respectively. For polarized photons and recoil polarization,

$$\begin{aligned}\frac{d\sigma}{d\Omega} &= \sigma_0[1 - P_{lin}\Sigma\cos 2\varphi \\ &+ P_{x'}(-P_{lin}O_{x'}\sin 2\varphi - P_\lambda C_{x'}) \\ &- P_{y'}(-P + P_{lin}T\cos 2\varphi) \\ &- P_{z'}(P_T O_{z'}\sin 2\varphi + P_\lambda C_{z'})].\end{aligned} \tag{2}$$

For polarized target and recoil polarization, the cross section can be expressed as

$$\begin{aligned}\frac{d\sigma}{d\Omega} &= \sigma_0[1 + P_{y'}P + P_x(P_{x'}T_{x'} + P_{z'}T_{z'}) \\ &+ P_y(T + P_{y'}\Sigma) - P_z(P_{x'}L_{x'} - P_{z'}L_{z'})].\end{aligned} \tag{3}$$

2.1.2 Polarized Deuteron Target

For the polarized beam and a polarized deuteron target, the cross section for single-pseudoscalar meson production can be expressed as

$$\begin{aligned}\frac{d\sigma}{d\Omega} &= \sigma_0[1 + P_\gamma^L\left(\Sigma + \frac{1}{\sqrt{2}}P_D^T T_{20}^L\right)\cos 2\varphi \\ &+ P_\gamma^L P_D^V G\sin 2\varphi \\ &- P_\gamma^C P_D^V E + \frac{1}{\sqrt{2}}P_D^T T_{20}^0].\end{aligned} \tag{4}$$

Here P_D^V is the vector polarization of the deuteron along the beam axis, P_D^T is the deuteron tensor polarization, P_γ^C and P_γ^L are the circular and linear photon polarizations, respectively, and φ is the angle between the linear photon polarization and the reaction plane. Two additional Tensor asymmetries T_{20}^L and T_{20}^0 can be measured by optimizing the tensor polarization of the spin-1 target while minimizing the vector polarization. In addition, the tensor polarization can be minimized when taking data for the vector polarization observables. The manipulation of vector and tensor

polarization using RF-irradiation has been the focus of recent solid polarized target research at the University of Virginia. This will be discussed further in Section 3.

For the case of polarized beams and an analysis of recoil hyperon polarization, the cross sections are

$$\begin{aligned} \frac{d\sigma}{d\Omega} &= \sigma_0[1 + P_\gamma^L\,(\Sigma - P_r^y T)\cos 2\varphi \\ &- P_\gamma^L\,(P_r^x O_{x'} + P_r^z O_{z'})\sin 2\varphi \\ &- P_\gamma^C\,(P_r^x C_{x'} + P_r^z C_{z'}) \\ &+ P_r^y P]. \end{aligned} \tag{5}$$

The dependence on target and recoil polarization is given by

$$\begin{aligned} \frac{d\sigma}{d\Omega} &= \sigma_0[1 - P_D^V\,(P_r^x L_{x'} - P_r^z L_{z'}) \\ &+ P_r^y P \\ &+ P_\gamma^L P_D^V\,(P_r^x T_{z'} - P_r^z T_{x'}\sin 2\varphi)]. \end{aligned} \tag{6}$$

2.2 Vector Mesons

There are many pseudoscalar meson channels that can be very interesting to study with a polarized target. The π, η, and η' are all lacking complete polarized target data at the Hall-D photon energy range, not to mention exotic baryon resonance search in $\gamma n \to K^- X$. Polarization effects in the photoproduction of the pseudoscalar $\bar{D}$ charmed mesons in exclusive processes $\gamma + N \to Y_c + \bar{D}$ with a circularly polarized photon should lead to nonzero polarization of the Y_c-hyperon with $x-$ and $z-$components and non vanishing asymmetries using a polarized target. There is much to study near threshold and very little polarized target data so far available.

2.2.1 ϕ-Mesons Production

Measurement of double polarization asymmetries for ϕ photoproduction with the polarized target and a polarized photon beam is a sensitive means to investigate small and exotic amplitudes, such as an $s\bar{s}$-quark content of nucleons via interferences with dominant amplitudes and the determination of the spin value of produced hadrons as the pentaquark. In order to realize the double polarization measurements to study the $s\bar{s}$-quark content as well as exotic hadron structures, the processes $\gamma p \to K^* Y$ and $\gamma p \to \phi p$ should be studied in the Hall-D accessible photon energy range. Some polarization observables in vector meson photoproduction are discussed here [11, 12].

For coherent photoproduction from the polarized deuteron using circularly-polarized photon-beam, there are three initial spin states with total spin projection: $J_z = 2$ when the deuteron is polarized along the beam polarization, $J_z = 0$ when the deuteron is polarized along the opposite direction to the beam polarization, and $J_z = 1$ when the deuteron is polarized perpendicular to the beam polarization. This leads to three beam-target asymmetries C_{BT}^{21}, C_{BT}^{20}, and C_{BT}^{10}. From [13], the amplitude of the photoproduction deuteron is proportional to the product of the elementary

isoscalar amplitude and the deuteron form factors, which differ for the processes with *natural* and *unnatural* parity properties. The amplitudes decrease fast with $-t$ due to the effect of these form factors. The unnatural parity-exchange transitions are suppressed for the deuteron in the tensor polarized target with spin projection $M_i = 0$. The form factors of the natural parity-exchange (Pomeron) amplitudes with spin projections $M_{i,f} = \pm 1$ and $M_{i,f} = 0$ are distinct and both differ from the *unnatural* parity-exchange form factor. Tensor target optimization applicable for these types of solid polarized targets is discussed in Section 3.

For the incoherent photoproduction from the deuteron, the total amplitude is a coherent sum of the photoproduction from the proton and the neutron. The interference term between these two amplitudes in a deuteron is proportional to the linear combination of the deuteron form factor. For the polarized deuteron target, there are three beam-target asymmetries analogous to the coherent photoproduction observables already mentioned. These can be used in combination with analysis of the photoproduction from the proton, leading to unique solutions to the exotic channels with unnatural parity exchange ($s\bar{s}$-knockout) in the photo-reaction with a neutron.

There are many ϕ meson production channels that are worthy of polarized target investigation at the Hall-D photon energies, such as $\gamma p \rightarrow \phi p$, $\gamma d \rightarrow \phi d$, $\gamma d \rightarrow \phi pn$. Hall-D can now cover the photon energy region not yet studied by past experiments. This data will be complimentary to Hall-B Frozen spin g8, g9, and HD-ice g14 at 6 GeV as well as the low q^2 12 GeV proposals on HD-ice along with the LEPS HD-ice data. Here we expect to cover a larger kinematic range with higher statistics than the present Hall-B proposal with high polarization for the proton and deuteron vector and tensor polarizations. In addition, greater sensitivity to the tensor polarized observables can be achieve with a RF-manipulated Frozen spin target.

2.2.2 ω-Mesons Production

The theoretical interpretation of cross-section data for $\gamma N \rightarrow \omega N$ [14, 15, 16, 17, 18] indicate dominant t-channel production from unnatural parity exchange (π^0 and possibly η) at low energies and natural parity exchange (pomeron) at higher energies, and sizeable nucleon u-channel contributions. The relative strength of competing natural and unnatural parity-exchange processes can in principle be extracted using plane-polarized photons [19], a project that is of particular interest in the photon energy range of Hall D, to map out the transition from unnatural to natural parity exchange. Additional target polarization provides double-polarization observables C_{BT}^{ij}, which are crucial when performing the separation in the presence of u-channel (nucleon-pole) contributions, with C_{BT}^{zy}, C_{BT}^{zz} changing signs in backward direction for u and unnatural parity exchange [20, 21]. Moreover, the observables C_{BT}^{xy}, C_{BT}^{xz} vanish for all production angles [21]. Detailed investigations of these contributions are feasible with the proposed polarized target inside the GlueX detector.

2.2.3 J/ψ-Mesons Production

A promising approach to studying polarized gluons in the nucleon is photoproduction of either open charm or inelastic J/ψ through the hard process of photon-gluon fusion $\gamma + gc\bar{c}$. Other mechanisms for producing charm are suppressed due to the mass of the charm quark. Open charm production can be understood in terms of the photon gluon fusion process. Higher order dia-

grams have been calculated for both the polarized [22, 23, 24] and unpolarized case [25, 26]. The asymmetry for J/ψ photoproduction has been calculated [27] and is proportional to a ratio of convolution integrals over $\Delta g(x)$ and $g(x)$. Exploring both the $\Delta g/g$ using photon-gluon fusion as well as the asymmetries of J/ψ in the low energy region have not yet been attempted.

Double spin asymmetries of the vector meson J/ψ around threshold may offer some insight on the polarized gluon distribution function in the nucleon. The measurement of J/ψ photoproduction asymmetries can be used to directly access the polarized gluon density [28] for larger s. However, data starting slightly below threshold reaching to slightly above would very much contribute to this study. In [28], it is argued that a measurement of the polarized gluon density via double spin asymmetries in charmonium photoproduction can potentially provide an additional test of the NRQCD FA, or alternatively, the polarized gluon distribution can be measured once the FA is confirmed. The double-spin asymmetry A_{LL} for inclusive J/ψ photoproduction is defined as

$$A_{LL}^{J/\psi}(\gamma p) = \frac{d\sigma(\overrightarrow{\gamma} + \overrightarrow{p} \to J/\psi + X) - d\sigma(\overrightarrow{\gamma} + \overleftarrow{p} \to J/\psi + X)}{d\sigma(\overrightarrow{\gamma} + \overrightarrow{p} \to J/\psi + X) + d\sigma(\overrightarrow{\gamma} + \overleftarrow{p} \to J/\psi + X}, \tag{7}$$

where the arrows over γ and p are the helicity projection on the direction of the corresponding momenta of the initial particles.

Naturally, the exclusive case can also be useful. In photoproduction of J/ψ on a polarized proton target, a finite polarization asymmetry should arise because of $c\bar{c}$ Fermi-motion and binding-energy effects. The asymmetry depends on the polarized non-forward gluon distribution of the proton and thus gives information on gluon polarization in the proton. Though these asymmetries are expected to be small, a nonzero measurement just above threshold over a large angular coverage would be a significant measurement.

2.3 Threshold Charm Production

Asymmetries can be used to measure helicity correlations near threshold to explore the spectrum for exotic states. The are no polarized target observables studied yet near threshold for photon energy of 7.7 GeV for $\gamma p \to \eta_c p$, 8.2 GeV for $\gamma p \to J/\psi$, or 8.7 GeV for $\gamma p \to \bar{D}\Lambda_c$. A worth experiment to assist the search for exotic resonances should produce high statistics data in different initial state helicity configurations as part of a comprehensive study of this largely unprobed energy region. In addition, pushing the photon energy range to explore as high as 10.3 GeV could be interesting for the sake of the $P_c(4380)$, though the cross section is likely to be extremely small. For physics of this nature, using a radiator without a tagger and a bender magnet in the form of a compact photon source in combination with a horizontal evaporation fridge with a polarized NH_3 target is the best way to optimize the figure of merit. In this way, photon intensity is only limited by detector sensitivity to radiation. The disadvantage is the loss of exclusivity in many channels provided by tagging the incoming photon.

The restrictions imposed on the $c\bar{c}$ production by the quantum numbers of the soft final state require taking into account soft gluons. In the color evaporation model (CEM), color interactions are treated by averaging over possible final states below the open charm threshold [29]. CEM has been reasonably successful in describing some data. In hadroproduction there are significant

polarization effects and an enhancement in $\sigma(\bar{p}A \to J/\psi X)/\sigma(pA \to J/\psi X)$ at low c.m. energies due to dominance of $\sigma(\bar{q}q \to gg \to J/\psi)$. In photoprodroduction CEM can accurately describe data over a wide range of photon energies but is not expected to be valid near threshold.

The color singlet model or CSM has had some success by including as many hard gluons as needed to fully implement the restrictions imposed by the final state [30]. The CSM has been applied to J/ψ photoproduction, but fails to reproduce the absolute normalization and large p_T dependence in hadronproduction. Strong, high P_T suppression comes in CSM from the hard propagators. The octet mechanism [31] incorporates effects of soft gluons from the final state with the CSM taking into account color octet $c\bar{c}$ configurations. In photoproduction, inclusion of color octet contributions leads to errors in cross section and values of the relevant color octet matrix elements.

At high energies, dominant contribution to photoproduction comes from the elastic, diffractive region where there are three subprocesses corresponding to the photon dissociation into $c\bar{c}$ pair, $c\bar{c}$ scattering of the nucleon, and formation of the bound charmonium. For threshold production in contrast to the high energy photoproduction, the nucleon is nearly at rest. Additionally, the net momentum fraction carried by the spectators is $x \sim 0$, and $c\bar{c}$ scattering probes the $(1-x) \sim 1$ configuration of the target wave function. Near threshold all kinematic variables $s \sim M_{cc}^2$, $|t| \sim |u| \sim m_N M_{c\bar{c}}$ are large compared to Λ_{QCD} so that it may be possible that production mechanisms are dominated by short distance effects. To transfer the entire target momentum to a single quark in leading twist, hard gluons must be exchanged between all of the constituents, which leads to the $(1-x)^{2n_s-1}$ behavior near $x \to 1$, where n_s is the number of spectators, known from DIS for Bjorken $x \to 1$. It is possible that there are subleading twist contributions coming from the intrinsic charm component of the target wave function that can be explored more explicitly in a polarized target experiment. The gluon spin density within the nucleon can be studied using the parallel/anti-parallel asymmetry for producing open charm. Significant constraints can be placed on the shape and magnitude of $\Delta g(x)$ for the threshold region. The asymmetry for J/ψ photoproduction has been calculated [27] and is proportional to a ratio of convolution integrals over $\Delta g(x)$ and $g(x)$. Near threshold testing should make an interesting study of $\Delta g/g$ by achieving high statistical precision as well as testing the reaction mechanism while studing a large kinematic range.

2.4 Other Mesons

These polarized target asymmetries could also be studied for K^* and D^* in a kinematic region that so far has very little data. Candidate vector mesons like the $Y(2175)$ can be explored using the polarized target observables to further constrain backgrounds. Results from these asymmetries can be used to help resolve supernumerary states from those that are not. A polarized target could lead to the first measurements of the transverse target asymmetry and beam-target asymmetry for many mesons in $\bar{\gamma}\bar{N} \to XN$ for the photon energy range 5-9 GeV.

2.5 Additional Polarized Spin-1 Observables

Several other reactions that can be studied using the polarized deuteron target which exploit the spin-1 vector and tensor polarization. One example is the single- and double-spin asymmetries for $\gamma d \to \pi^- + p + (p)$ at large $t = (p_\gamma - p_\pi)^2$. Separation of S and D wave can be explored in this

scattering process with a tensor polarized deuteron. To simplify the dynamics one needs $-t \geq 2$ GeV^2. This process is sensitive in well defined kinematics to nuclear transparency effects [32, 33]. Another interesting direction is production with polarized deuteron with coherent recoil which has much stronger sensitivity to double scattering than the unpolarized case with effects being large already at $t \sim 0.5$ GeV^2. In addition, one of the most fundamental processes on the polarized deuteron is two-body photodisintegration $\gamma + d \to p + n$, which can easily be studied in Hall-D covering a large region of center of mass angle. Several important observables still are measured with insufficient accuracy or not measured at all. Similarly to the tensor asymmetries mentioned in vector and pseudoscalar meson production, the tensor polarized deuteron observables in two-body photodisintegration are among the most poorly known. Polarization observables are expected to be sensitive to important dynamical details and thus allow in general much more stringent tests of theoretical models. The tensor polarizations are especially interesting because there is a correlation between the degree of tensor polarization and the spatial alignment of the deuteron. This correlation is associated with the difference in partonic constituency through quark distributions. In this way, the deuteron provides the ideal tool for exploring the transition between nuclear and quark-gluon description of hadrons. Spatial alignment of the target deuterons can lead to large asymmetries in final state interactions in photodisintegration. In addition, the angular distribution of the pn pair in the final state for different polarizations can be very sensitive to the short range structure of the deuteron.

Following the notation of Schmitt and Arenhoevel[34], the polarization observables can be seen in the cross section of the two-body photodisintegration of the polarized deuteron (unpolarized photon) can be expressed as

$$\begin{aligned} \frac{d\sigma}{d\Omega} &= \frac{d\sigma_0}{d\Omega}\{1 - \sqrt{3/4}P_z \sin\theta_{d\gamma} \sin\phi T_{11}\left(\theta_p^{cm}\right) \\ &+ \sqrt{1/2}P_{zz}[(3/2\cos^2\theta_{d\gamma} - 1/2)T_{20}\left(\theta_p^{cm}\right) \\ &- (\sqrt{3/8}\sin 2\theta_{d\gamma}\cos\phi T_{21}\left(\theta_p^{cm}\right) \\ &+ (\sqrt{3/8}\sin^2\theta_{d\gamma}\cos 2\phi T_{22}\left(\theta_p^{cm}\right)]\}, \end{aligned} \tag{8}$$

where σ_0 is the unpolarized cross section, P_z (P_{zz}) is the degree of vector (tensor) polarization, $\theta_{d\gamma}$ is the angle between the polarization axis and the momentum of the γ-quantum, and ϕ is the angle between the polarization plane and the reaction plane. The tensor analyzing powers T_{2I} are functions of photon energy E_γ and proton emission angle θ_p^{cm}. Tensor polarization of deuterons and its optimization for scattering experiments is discussed in detail in Section 3.

The most basic theoretical prediction would extend the calculation [34] to higher energy using a one-body current given the Bonn OBEPR NN potential with the major part of meson exchange currents (MEC). After adding the pion exchange currents ("+MEC"), isobar configurations ("+IC") and the leading order relativistic corrections ("+RC") can then be added. The calculation of [35] includes heavy-meson and all MEC diagrams with isobar configurations, and relativistic corrections can be used for relavent photon energy. The deuteron PD above pion production threshold is investigated in [36] in a coupled-channel approach with $N\Delta$ and πd channel, using a dynamic treatment of the pions. As a result, the NN potential and $\pi - MEC$ become retarded and electro-

magnetic loop corrections are included. A complete theoretical description for the correct photon energy range is needed.

2.6 Dyson-Schwinger Equation

It is possible to make direct calculations of exotic spectra using the Dyson-Schwinger Equation (DSE), either as $q\bar{q}$ states or as tetraquarks. Exotic quantum numbers can exist as $q\bar{q}$ states (but don't have a "nonrelativistic limit"). Recent work in calculations using DSE find exotic quantum number in $q\bar{q}$ to which the helicity amplitudes can be incorperated leading to difference observables which help to distiguish them in the spectrum. It is now possible to go beyond rainbow-ladder truncation and calculate all quantum numbers, ground and excited states, light and strange quarks. This work is presently underway [37].

In photoproduction, at the hadronic level, for the hadronic exchange terms that enter the process, extraction of the couplings of exotics to NN* could be studied, as well as the π-γ-exotic transition form factors from the t-channel exchange. To extract these numbers with sufficient precision would require polarized target observables. This is something that can be calculated using the DSE [37] as a transition form factor from the nucleon to a resonace, which couple to a current with exotic quatum numbers in the timelike region with the exotic meson onshell. With these calculations and experimental data much insight could be gained into the nature of what exotics are.

2.7 Compton Scattering

Significant progress has been made over the last decade in our understanding of exclusive reactions in the hard scattering regime. This progress had been made possible (in part) by data from Jefferson Lab on elastic electron scattering and Compton scattering from the proton, and by a significant and increasingly sophisticated theoretical effort to exploit the richness of exclusive reactions at moderate momentum transfers.

The observation of scaling in Deep Inelastic Scattering (DIS) at relatively low momentum transfers, successfully understood within the framework of pQCD, suggested that the same interpretation would be fruitful when applied to exclusive reactions: elastic electron scattering, photo- and electro-production of mesons, and Compton scattering. This prospect was further supported by the fact that constituent counting rules [38, 39], which naturally govern reactions that conform to the pQCD picture, could describe certain exclusive reactions.

There is little doubt that the pQCD mechanism dominates at high energies. What has been lacking is a general agreement as to how high the energy must be for pQCD to be completely applicable. The argument on this point is driven by more than a difference of (theoretical) opinion. The unavoidable fact is that cross sections calculated in a pQCD framework have invariably been low when compared to data, sometimes by an order of magnitude or more [40].

Results of the following experiments performed at Jefferson Lab on the proton contradict the predictions of pQCD: the recoil polarization measurements of G_p^E, E93-027, E04-108, and E99-007, and the Real Compton Scattering (RCS) experiment E99-114. The G_p^E measurements [41, 42, 43] found that the ratio of F_2 and F_1, scaled by Q^2, demands a revision of one of the precepts

of pQCD, namely hadron helicity conservation. Results from the RCS measurement [44] show that the longitudinal polarization transfer K_{LL} is large and positive, also contrary to the pQCD predictions which find K_{LL} to be small and negative. These two experiments provide a compelling argument that pQCD should not be applied to exclusive processes at energy scales of 5-10 GeV.

Fortunately, an alternate theoretical framework exists for the interpretation of exclusive scattering at intermediate energies [45, 46, 47]. This alternative approach asserts the dominance of the handbag diagram in which the reaction amplitude factorizes into a subprocess involving a hard interaction with a *single quark*. The coupling of the struck quark to the spectator system is described by the Generalized Parton Distributions (GPD's) [48, 49]. Since the GPD's are independent of the particular hard scattering reaction, the formalism leads to a unified description of hard exclusive reactions. Moreover, the relationship between GPD's and the normal parton distribution functions provides a natural framework for relating inclusive and exclusive reactions.

The RCS experiment E99-114 produced an especially remarkable result; not only was the measurement of K_{LL} inconsistent with pQCD, it was found that the longitudinal polarization is nearly as large as that expected for scattering from a free quark.

The QCD factorization approach formulated in the framework of Soft Collinear Effective Theory (SCET) can be used to develop a description of the soft-spectator scattering contribution [50, 51, 52]. Recently, a derivation of the complete factorization for the leading power contribution in wide angle Compton scattering has been worked out in the soft collinear effective theory. As factorization evolves and becomes less dependent on the assumption of restricted parton virtualities and parton transverse momenta, RCS should receive the same level of attention that DVCS has. RCS have a complementary nature to DVCS in so far as that in DVCS the GPDs are probed at small t, while for RCS (and nucleon form factors) the GPDs are probed at large t.

A formalism for the RCS process based on the Dyson-Schwinger Equation (DSE) approach has been proposed by G. Eichmann and C. Fisher [53]. The specific results for the WACS observables in this framework are not yet published.

The initial state helicity correlation can be used to probe a theoretical model in detail. According to the handbag approach, their angle dependence is close to that of the subprocess $\gamma q \to \gamma q$ diluted by form factors which take into account that the proton is a bound state of quarks and which represent $1/x$ moments of GPDs. The electromagnetic nucleon form factors have been revised using the generalized parton distributions analysis by M. Diehl and P. Kroll [54]. The various theoretical efforts made to apply the handbag approach to wide angle compton scattering (WACS) have produced predictions for its polarization observables, including K_{LL} and A_{LL} [46, 55]. We must emphasize that the results of E99-114 are at a single kinematic point of a single observable. It is essential to verify the dominance of the handbag mechanism in other observables such as A_{LL}. In a recent development [55], a calculation of Miller suggests that a measurement of A_{LL} in WACS would be a test of perturbative chiral symmetry and of the mass of the quarks participating in the hard scattering.

Within the SCET framework it is possible to relate the polarized observables only in the large angle kinematics $-t \sim -u \geq 2.5$ GeV^2. The SCET formalism follows the same idea as in the standard factorization approach, short and long distance physics are factorized separately. The only required assumptions are very general such that soft partons have soft momenta of order Λ_{qcd}.

There is not an additional need to constrain the virtualities by hand. The advantage of SCET formalism is a systematic approach to the factorization of the hard and soft subprocesses. Along with comparing the difference of A_{LL} and K_{LL} over a spread of angles, any measurement of K_{LL} at different photon energies provides additional constraints given the s-dependence predicted. The GPD model and SCET approach predict that $K_{LL} = K_{LL}(KN)$ at leading-order (KN asymmetry). This implies not only specific angular behavior but also dependence on s. In the SCET framework there are also α_s corrections which induce a weak logarithmic dependence. A measurements at the same angle and different s allow one to check the expected theoretical prediction and to make a conclusion about our understanding of the underlying scattering of quarks.

There is much theoretical interest in WACS and much new data required. The polarized observables are essential for moving the framework forward. There was only one polarization measurement of K_{LL} made during E99-114, so a similar experiment (E07-002) [56] at higher s was undertaken in Hall-C resulting in an additional K_{LL} point [57]. These are both relatively remarkable measurements in that they are inconsistent with predictions based on the pQCD theory and hence suggests that the asymptotic regime for the WACS process in not yet kinematically understood. Such a large K_{LL} could be caused by noncollinear effects in exclusive reactions at currently accessible energies and parton correlations in the nucleon. In this respect, the K_{LL} increase may be related to significant roles observed in elastic electron-nucleon scattering of both quark orbital angular momentum and a u-d diquark correlation [58, 59, 60, 61, 62, 63]. The GPD model and the SCET approach both predict that $K_{LL} = K_{LL}(KN)$ at leading order (KN asymmetry). This implies not only specific angular behavior but also independence on s. In the SCET [52] framework there are also α_s corrections which induce a weak logarithmic dependence. Measurements at the same angle and different s allow one to check the expected theoretical prediction and to make a conclusion about the our understanding of the underlying scattering process of the quarks.

In addition sub-leading helicity flip amplitudes can provide a sizable numerical effect at small angles even if the ratio of helicity flip amplitudes to helicity conserving amplitudes is similar to the behavior G_E/G_M. Many angle and energy are need with large mandelstam variables. In this way the measurements of A_{LL} can help to clarify the role of the power suppressed helicity flip contributions in WACS and help to understanding the hard reaction mechanism. In SCET framework A_{Ll} measurements will allow direct extraction of information about helicity flip amplitudes. The small cross section at large s would imply a very long Hall-D run, but decent statistics at lower s for a large angle coverage will be collect by configuring a trigger for Compton scattering while any of the other longitudinally polarized target data is being collected. With a dedicated effort and the BDT to separate single and background, Hall-D could obtain unprecedented kinematic coverage of A_{LL} as well as the transverse polarized target observables A_{LS} and A_{LN} in Compton scattering at energies 5-9 GeV. The longitudinal and transverse polarized observables can all so be achieved for Time-like Compton scattering in the same Hall D experiment.

2.8 Spin-Dependent Total Cross Sections

It is also possible to measure the spin-dependent total cross section for circularly/linearly polarized photons absorbed on longitudinally/transverse polarized protons or neutrons over the Hall-D photon energy range. This would be the first measurement of the difference between left- and

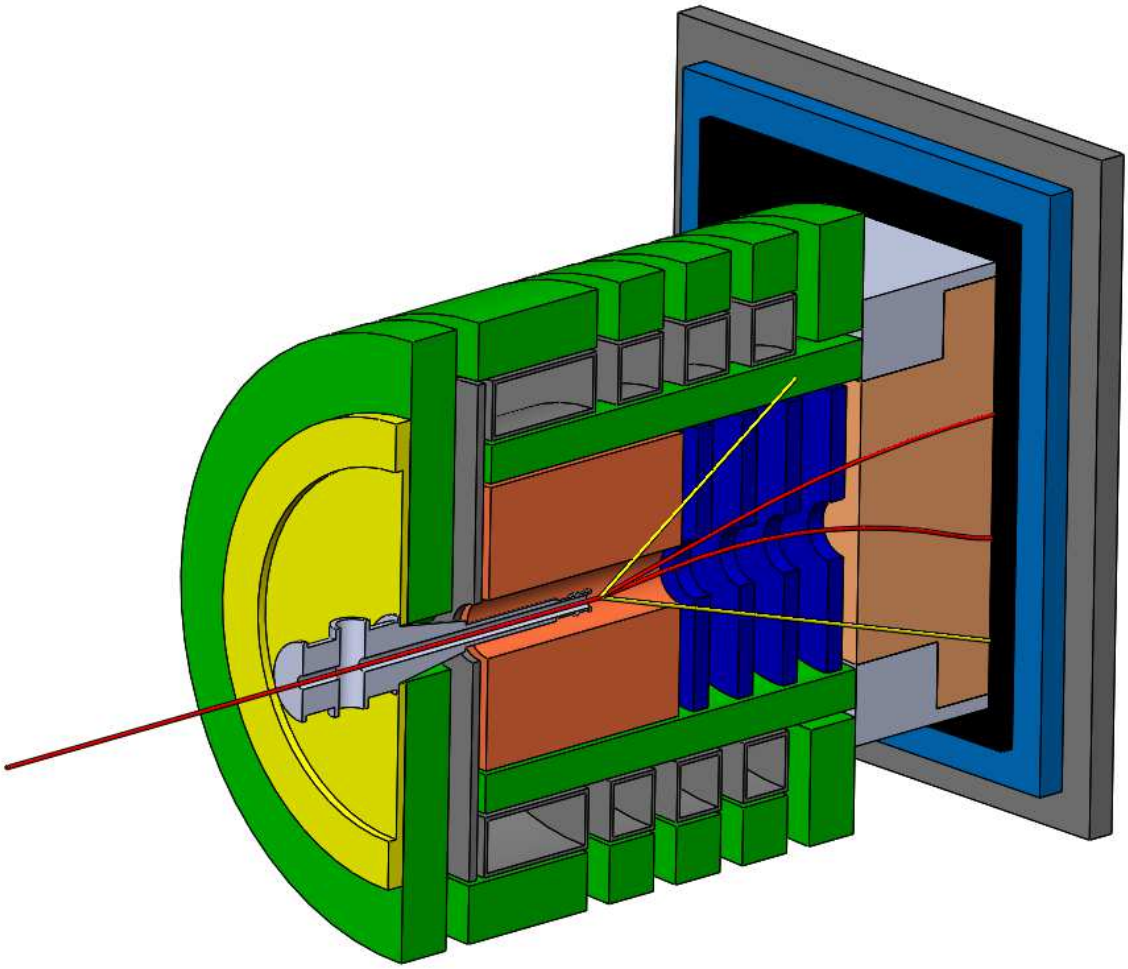

Figure 1: A Frozen Spin Target fitted into GlueX.

right-handed polarized photoproduction above the resonance region. This would help to build an understanding of the high energy convergence of the fundamental Gerasimov-Drell-Hearn sum rule for the proton and neutron. Contributions would be expected in the GlueX accessible kinematics, especially for the isovector combination. Measurements of the magnitude and energy-dependence of the polarized photo-absorption could also provide information to enhance the understanding of soft Regge physics.

3 The Polarized Target

The experimental program will utilize a new frozen spin polarized target of protons and deuterons specifically constructed for operation with the Hall D infrastructure and the GlueX detector package, see Fig. 1. A frozen spin target in Hall D has also been examined for another proposed experimental program [64]. The most likely target material will be butanol (C_4H_9OH) or deuter-

ated butanol (C_4D_9OD) in the form of 1–2 mm frozen beads filling a target cell 2 cm in diameter and about 7 cm long. The material will be dynamically polarized using a separate, warm bore, 5 T superconducting solenoid located upstream of the Hall D solenoid. Once polarized, the target cryostat will be extracted from the 5 T magnet and moved to the center of the Hall D solenoid, a distance of a few meters.

Scattering data will be acquired while the target polarization decays in an exponential manner with a 1/e time constant T_1 that depends strongly on both the sample temperature and the strength of the magnetic holding field. A high power ^{3}He-^{4}He dilution refrigerator will be employed to cool the material to about 0.3 K during dynamic polarization and below 50 mK during data acquisition. A thin 0.5 T superconducting solenoid will be installed inside the cryostat to maintain the polarization during transport. The 1.8 T field of the Hall D solenoid will then be used to hold the polarization during the longitudinal portion of the experimental program. The 0.5 T transport coil will be replaced by a saddle coil of similar strength for the transverse measurements. In this case, the longitudinal field of the Hall D solenoid must be shielded from the target. In Section 4 we demonstrate that a shielding magnet can be used to zero an external field.

A frozen spin target (FROST) similar to the one envisioned here, was constructed for the CLAS spectrometer in Hall B [65]. A frozen spin target is shown in Fig. 2. Proton polarizations of 95% were achieved in this system with butanol samples doped with the paramagnetic radical TEMPO, with T_1 values up to 4000 h at temperatures less than 25 mK and holding fields of approximately 0.5 T. The target was repolarized about once per week, a process that required a maximum of approximately 8 hours. In a single test with FROST, a record deuteron polarization of -87% was demonstrated in deuterated propanediol ($C_3D_8O_2$) doped with the recently developed trityl radical OX065 (see Figure 3). The deuteron relaxation time was not measured during this test, but relaxation times of1500 h have been observed in the Mainz frozen spin target [66] under similar conditions. T_1 values exceeding 10,000 h should be realized when the 1.8 T Hall D solenoid is used to hold the polarization.

3.1 Tensor Polarization Manipulation

When a spin 1 system such as the deuteron is subjected to a magnetic field along the z-axis, the Zeeman interaction gives rise to three magnetic sublevels $I_z = +1, 0, -1$ with population fractions p_+, p_-, p_0, respectively. These populations are described by both a vector polarization,

$$\begin{aligned} P_z &= \langle I_z/I \rangle \\ &= (p_+ - p_0) + (p_0 - p_+) = p_+ - p_-, \end{aligned} \tag{9}$$

and a tensor polarization [67],

$$\begin{aligned} P_{zz} &= \langle 3I_z^2 - I(I+1) \rangle / I^2 \\ &= (p_+ - p_0) - (p_0 - p_-) = 1 - 3p_0, \end{aligned} \tag{10}$$

which are subject to the overall normalization $p_+ + p_- + p_0 = 1$.

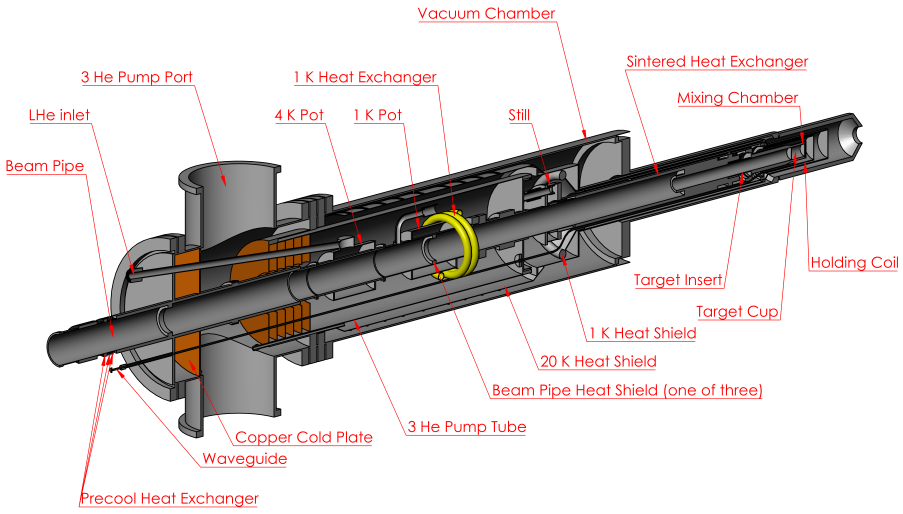

Figure 2: Cross section view of a FROST target fridge, with the overall length of the cryostat is approximately 2 m.

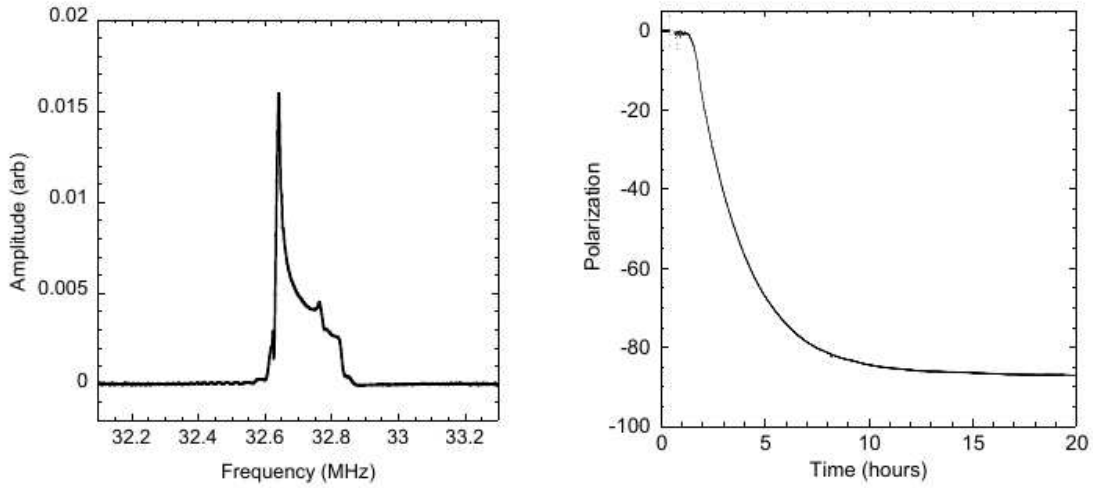

Figure 3: Performance of the signal and polarization growth curve of deuterated propanediol doped with OXO63 from Jlab Hall-B FROST experiment.

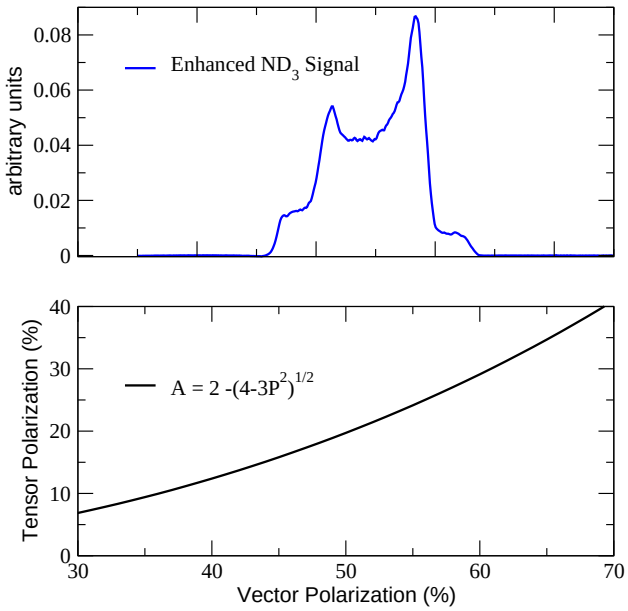

Figure 4: **Top**: NMR signal for ND_3 with a vector polarization of approximately 50% from the GEN experiment. **Bottom**: Relationship between vector and tensor polarization in equilibrium, and neglecting the small quadrupole interaction.

In the case of deuteron spins in thermal equilibrium with the solid lattice, and neglecting the small quadrupole interaction [67], the three substates are populated according to Boltzmann statistics and the tensor polarization can be related to the vector polarization via

$$P_{zz} = 2 - \sqrt{4 - 3P_z^2}. \tag{11}$$

The maximum absolute value of $P_{zz} = -2$ occurs only for vanishing populations in the $m = \pm 1$ states. If, on the other hand, only the $m = 1$ or $m = -1$ state are occupied, the vector polarization reaches its maximum value of $+1$, and $P_{zz} = +1$. For positive tensor polarization A where the spins are in Boltzmann equilibrium the tensor and vector relationship is show in Fig. 4.

It is the requirement that one has a very high degree of vector polarization in order to obtain a possibly useful degree of tensor polarization. The experimental tensor target asymmetry can be achieved using three different helicity configurations. This is expressed as

$$a_T = \sqrt{2}\left(\frac{N^+ - N^-}{P_{zz}^+ N^- - P_{zz}^- N^+}\right) = \sqrt{2}\left(\frac{N^+ - N}{P_{zz}^+ N}\right) = \sqrt{2}\left(\frac{N^- - N}{P_{zz}^- N}\right), \tag{12}$$

where $N^+(N^-)$ is the number of events detected with positive (negative) target polarization and N is the number of events detected with an unpolarized target. The tensor asymmetry can be found using positive and negative tensor polarization, using just positive tensor polarization and an unpolarized target, or using just negative tensor polarization and an unpolarized target. With the goal of mitigating the vector polarization, it is most convenient to use a negatively tensor-polarized target and an unpolarized target.

Deuteron spin alignment can be manipulated when exposed to a modulated RF field using an external coil around the target cup. The accuracy and enhancement of the tensor polarization is greatly dependent on the polarization technique. Tensor polarization can be measured when the magnetic sublevels are out of the Boltzmann distribution, when the intensities I_+ and I_- of each peak in the NMR signal represent the total area of each independent transition probability distribution. The tensor polarization under any spin distribution can be described as

$$P_{zz} = C(I_+ - I_-). \tag{13}$$

Here C is the calibration constant. A positive tensor polarization enhancement occurs only when the $n_+ + n_-$ population increases with respect to n_0 population. To optimize positive tensor polarization, the vector polarization must be maximized using DNP, at which point the microwave is turned off and the RF-modulation begins. The RF-modulation induces transition at the frequency domain that it spans. Tensor polarization optimization will occur when the range in RF-modulation is chosen to maximize the difference in the intensities I_+ and I_- throughout the signal.

Negative tensor enhancement can be achieved by proton deuteron cross-polarization which fills the $m = 0$ sublevel directly from the spin reservoir of another (proton) system [68]. The deuteron spin system is polarized using strong thermal contact between the proton spin-spin interaction reservoir and the deuteron quadrupole interaction reservoir. The thermal contact is maintained using high powered RF just off of the Larmor frequency of the two spin species. As the $m = 0$ sublevel is filled, there are transitions of equal likelihood to the greater or lesser energy levels, so the NMR signal using this type of cross polarization has both absorption and emission. The greater the proton spin-spin reservoir, the greater the tensor polarization achievable in the deuteron. This can be done to achieve a near zero vector polarization, however the maximum tensor polarization that can be acquired for the thermal conditions of the Duke/UVA cryostat has yet to be studied. Measuring and fitting techniques for RF manipulated deuteron NMR lines have been recently developed at UVA.

A selective AFP (Adiabatic Fast Passage) can also be used to achieve negative tensor polarization. An AFP [69, 70] is a reverse in the polarization using a single RF sweep which is slow enough to follow the Adiabatic Theorem but is still fast with respect to the relaxation rates of the material at the temperature and field conditions. The spins effectively follow the magnetic field of the RF sweep as it passes through the resonance line, resulting in a helicity flip of the target. A selective AFP is when the RF is swept through a specific frequency domain to selectively manipulate the deuteron alignment. UVA has recently achieved this with d-butanol at 5 T and 1 K.

Negative tensor polarization is especially interesting because not only is it easier to hold zero vector polarization, but the magnetic sublevels $m = +1$ and $m = -1$ are depleted to both fill the $m = 0$ sublevel, leading to a magnetization reservoir that is twice as large. This doubling of the polarization reservoir is only useful when the target state can be held long enough to take data in an experiment. This is easily achieved when using a Frozen Spin Target where the temperature of the material is held below 100 mK, which slows the relaxation rates, effectively freezing the polarization in place.

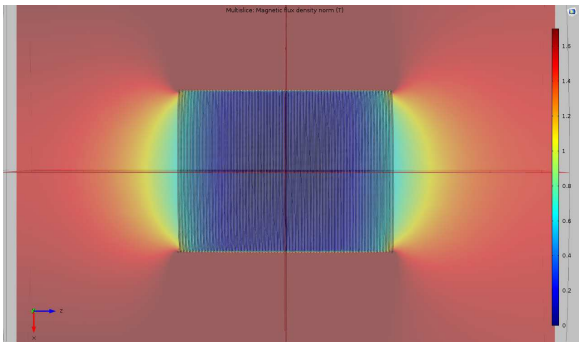

Figure 5: A shielding magnet used to zero out an external field of 1.8 T with a slight field gradient using COMSOL Multiphysics Simulation Software.

4 Holding Magnets

The longitudinal holding magnet can be built to cover a target of several centimeters long. The coil can be made with compensation end winding of 3 layers of ~ 0.1 mm multifiliment NbTi to assist the already existing semi-solenoidal magnetic field. The goal homogeneity over the target cell is about $\Delta B/B < 1 \times 10^{-}3$.

The transverse polarized target in the middle of the Hall-D semi-solenoidal magnetic field requires a non-conventional holding magnet constructed to counteract the semi-solenoidal magnetic field and generate a field around 0.6 T with homogeneity over the target cell of about $\Delta B/B < 5 \times 10^{-}3$. This must be done with different layers used to insulate the target space from the external semi-solenoidal field. The transversely polarized frozen spin target, which will include an additional compensation magnet to shield the target region so the transverse target magnet can operate. The magnetic system comprises of the frozen spin holding field saddle coil with the compensating solenoid, and a Helmholtz coil. A similar shielded configuration is intended to be used for the CLAS12 transverse target as well as for the transverse polarized target at the PANDA Experiment at FAIR. In figure 5 we demonstrate how a shielding magnet can be used to zero out an external field of 1.8 T using a DC coil simulation in COMSOL Multiphysics Simulation Software. A slight gradient (~ 0.25T/m) is included in the external field. The length used is 20 cm with a diameter of 15 cm.

Alternatively, in the case of the transverse field it's possible to reduce the large external polarizing magnet to the size of the internal holding coil with a much stronger field (~ 2.5 T). This is done by making the magnet coil as thin as possible (minimize absorption) with equal homogeneity. This is much easier to accomplish in a high powered dilution fridge. This type of design is being implemented in the Mainz frozen spin target at MAMI.

5 Summary

There is good reason to further consider the development of a polarized target for GlueX to study a broad range of polarized observables in the photon beam energy range between 5 GeV and

9 GeV. Both a polarized proton and a polarized deuteron target with both linear and circularly polarized photon beams have much physics to offer. A frozen spin target capable of longitudinal and transverse polarization offers the most physics. In this way it is necessary to design the fridge and magnets for optimal kinematic coverage to work with the Hall-D configuration of GlueX. A large set of polarization observables will be determined in a single experiment, including single-polarization and beam-target, target-recoil and beam-recoil double-polarization asymmetries, as well as tensor polarized observables, and initial state helicity correlations in possible exotic state hadrons. This experiment is complimentary to previously proposed GlueX experiments providing additional information to be used to determine compete isospin amplitudes and assist the search for exotic state mesons.

References

[1] S. J. Brodsky, Private Communication (2016).

[2] S. Brodsky, E. Chudakov, P. Hoyer, and J. Laget, SLAC-PUB **8677**, (2000).

[3] S. Brodsky, C. Ji, and G. Lepage, Phys. Rev. Lett. **51**, 83 (1983).

[4] Y. Oh, Y. Nakayama and H. Haberzett, Few-Body Systems **54**, 1251 (2013).

[5] Y. Nakayama, K. Oh and H. Haberzett, Phys. Rev. C **85**, 042201 (2012).

[6] W. Roberts and T. Oed, Phys. Rev. **C71**, 055201 (2005).

[7] W. Ochs, Nuovo Cim. **A12**, 724 (1972).

[8] P. Estabrooks and D. Martin, Phys. Lett. **B41**, 350 (1972).

[9] B. Hyams, Nucl. Phys. **B64**, 134 (1973).

[10] G. Knochlein, D. Drechsel, and L. Tiator, Z. Phys. **A352**, 327 (1995).

[11] W. Pichowsky, S. Cetin, and F. Tabakin, Phys. Rev. **C53**, 593 (1996).

[12] W. M. Kloet, W.-T. Chiang, and F. Tabakin, Few-Body Systems Suppl. **11**, 308 (1999).

[13] A. Titov, M. Fujiwara, and L. T-S.H., Phys. Rev. **C 66**, 0222202 (2002).

[14] J. Ballam and others (ABBHHM Coll.), Phys. Rev. **D7**, 3150 (1973).

[15] R. W. Clift and others (LAMP. Coll.), Phys. Rev. **B72**, 144 (1977).

[16] D. P. Barber and others (LAMP2. Coll.), Z. Phys. **C26**, 343 (1984).

[17] J. Barth and others (SAPHIR Coll.), Eur. Phys. J. **A18**, 117 (2003).

[18] M. Williams and others (CLAS Coll.), Phys. Rev. **C80**, 065208 (2009).

[19] P. S. K. Schilling and G. Wolf, Nucl. Phys **B15**, 397 (1970).

[20] C. S. M. Pichowsky and F. Tabakin, Phys. Rev. **C53**, 593 (1996).

[21] A. I. T. Y. Oh and T.-S. H. Lee, Phys. Rev. **C63**, 025201 (2001).

[22] I. Bojak and M. Stratmann, Phys. Lett. **B433**, 411 (1998).

[23] I. Bojak and M. Stratmann, Nucl. Phys. **B540**, 345 (1999).

[24] Z. Merebashvili, A. Contogouris, and G. Grispos, hep-ph/0007050 .

[25] J. Smith and W. van Neerven, Nucl. Phys. **B374**, 36 (1992).

[26] R. K. E. Ellis and P. Nason, Nucl. Phys. **B312**, 551 (1989).

[27] G. M. and E. Reya, Z. Phys. **C39**, 569 (1988).

[28] G. Japaridze, W. Nowak, and A. Tkabladze, DESY **99-110**, 1 (1999).

[29] J. Amundson, O. Eboli, E. Gregores, and F. Halzen, Phys Lett **B390**, 323 (1997).

[30] M. Mangano, in proceedings of the Topical Workshop on Proton-Antiproton Collider Physics **Batavia, IL**, (1995).

[31] G. Boldwin, E. Braaten, and G. Lepage, Phys. Rev **D51**, 1125 (1995).

[32] L. Frankfurt, E. Piasetzky, M. Sargsian, and M. Strikman, Phys. Rev. **C51**, 890 (1995).

[33] L. Frankfurt, E. Piasetzky, M. Sargsian, and M. Strikman, Phys. Rev. **C56**, 2752 (1997).

[34] K.-M. Schmitt and H. Arenhoevel, Few-Body Syst. **7**, 95 (1989).

[35] M. Levchuck, Few-Body Syst. **19**, 77 (1995).

[36] M. Schwamb and H. Arenhoevel, Nucl. Phys. **A 696**, 556 (2001).

[37] G. Eichmann, Private Communication .

[38] S. Brodsky and G. Farrar, Phys. Lett. **31**, 1153 (1973).

[39] V. Matveev, R. Muradyan, and A. Tavkheldize, Lett. Nuovo Cimento **7**, 719 (1973).

[40] C. Bourrely and J. Soffer, Eur. Phys. J. **C36**, 371 (2004).

[41] M. Jones, Phys Rev. Lett. **84**, 1398 (2000).

[42] O. Gayou, Phys. Rev. Lett. **88**, 092301 (2002).

[43] A. Puckett, Phys. Rev. Lett. **104**, 242301 (2010).

[44] D. Hamilton, .

[45] A. Radyushkin, Phys. Rev. **D58**, 114008 (1998).

[46] H. Huang, P. Kroll, and T. Morii, Eur. Phys. J. **C 23**, 301 (2002).

[47] F. Cano and J. Laget, Phys. Lett. **B 551**, (2003).

[48] X. Ji, Phys. Rev. Lett. **78**, 610 (1997).

[49] A. Radyushkin, Phys. Lett. **B380**, 417 (1996).

[50] N. Kivel and M. Vanderhaeghen, JHEP **1304**, 029 (2013).

[51] N. Kivel and M. Vanderhaeghen, .

[52] N. Kivel and M. Vanderhaeghen, Eur. Phys. J. **C75**, 483 (2015).

[53] G. Eichmann and C. Fischer, Phys. Rev. **D 87**, 036006 (2013).

[54] P. Diehl, M. Kroll, Eur. Phys. J. **C73**, 2397 (2013).

[55] G. Miller, Phys. Rev. **C 69**, 052201 (2004).

[56] A. Nathan, R. Gilman, and B. Wojtsekhowski, JLab Experiment **E07-002**, .

[57] C. Fanelli *et al.*, Phys. Rev. Lett. **115**, 152001 (2015).

[58] G. Cates, C. de Jager, S. Riordan, and B. Wojtsekhowski, Phys. Rev. Lett. **106**, 252003 (2011).

[59] C. Roberts, M. Bhagwat, A. Hll, and S. Wright, J. Spec. Top. **140**, 53 (2007).

[60] I. Clot, G. Eichmann, B. El-Bennich, T. Klhn, and C. Roberts, Few-Body Syst. **46**, 1 (2009).

[61] M. Jones *et al.*, Phys. Rev. Lett. **84**, 1398 (2000).

[62] G. Miller, Phys. Rev. C **66**, 032201(R) (2002).

[63] O. Gayou *et al.*, Phys. Rev. Lett. **88**, 092301 (2001).

[64] C. Keith, **KL2016**, 223 (2016).

[65] C. Keith *et al.*, Nucl. Instru. and Meth. A **684**, 27 (2012).

[66] A. Thomas *et al.*, Physics of Particles and Nuclei **44**, 964 (2013).

[67] W. Meyer *et al.*, Nucl. Instrum. Meth. **A244**, 574 (1986).

[68] W. de Boer, Cern Report CERN-74-11 (1974).

[69] P. Hautle, PhD. Thesis.

[70] P. Hautle *et al.*, Nucl.Instrum.Meth. **A356**, 108 (1995).